Infections

Bernard F. Laya

Contents

B.F. Laya, M.D., DO
Institute of Radiology, St. Luke's Medical Center – Global City,
32nd Street, Bonifacio Global City, Taguig City 1634, Philippines
e-mail: bernielaya@aol.com

13.1   Introduction

Lower respiratory tract infection is the most common cause of illness in children and is a significant cause of morbidity and mortality. There are also associated complications, which should be recognized in order to make correct decisions regarding interventions or management. Clinical signs and symptoms are nonspecific, especially in infants and younger children. Some children with pneumonia even present with nonrespiratory symptoms including fever, malaise, decreased appetite, irritability, weakness, chest pain, and abdominal symptoms. Physical examination is also less reliable in children than adults (Donnelly 2001). Microbiological tests are important but could be difficult to obtain especially in younger children. Various medical imaging modalities not only play an important role as an aid in diagnosis but can also help during and after therapy. Diagnosis of pneumonia calls for a combination of clinical awareness, appropriate microbiological tests, and radiological studies.

13.2   Etiology

The cause of pneumonia in a child is often difficult to identify, but the patient's age can help narrow the possible etiologies. Viral pneumonia is rare in the neonatal period because of conferred maternal antibody protection. Group B streptococcus and Gram-negative enteric bacteria are the most common pathogen in neonates (birth to 20 days), obtained through vertical transmission from the mother during birth. From age 3 weeks to 3 months, *Streptococcus pneumoniae* is the most common pathogen. Viruses are the most frequent cause of community-acquired pneumonia in infants older than 4 months and in preschool-aged children, with respiratory syncytial virus (RSV) being the most common. For school-aged children (6–16 years old), the incidence of bacterial infections from *Streptococcus* increases, although viral disease remains the most common cause (Condon 1991; Ostapchuk et al. 2004). Bacterial pneumonia can occur at

any time in preschool and school-aged children and adolescents. *Mycoplasma pneumoniae* causes 30 % of lower respiratory tract infections in school-aged children (Condon 1991; Donnelly 2001). Infectious agents causing pneumonia are not limited to viruses and bacteria, but it could also be due to *Mycobacteria*, fungi, protozoa, and parasites. Co-infection with two or more microbial agents can also occur.

13.3   Imaging

Evaluation of suspected pulmonary infection is a very common indication for an imaging study in children. The role of imaging including chest radiographs, ultrasound, computed tomography (CT), and even magnetic resonance imaging (MRI) is to detect the presence or exclusion of pneumonia, determine its location, characterize and describe the extent of pneumonia, exclude other causes of respiratory symptoms, and show complications. It is also an important tool for image-guided interventions.

13.3.1 Chest Radiograph

The cornerstone of imaging in children suspected of having pulmonary infection is the chest radiograph. The radiographic appearance reflects the pathologic process occurring in the respiratory system (Bramson et al. 2005). Frontal and lateral views are obtained when possible because hyperinflation and lymphadenopathy are more accurately evaluated on a lateral radiograph especially in younger children. Lateral decubitus views may be useful in distinguishing free flowing pleural fluid versus loculated fluid collections. Chest radiographs have inherent limitations, but despite of this, there is moderate evidence to suggest that chest radiographs are sufficiently sensitive and highly specific for the diagnosis of community-acquired pneumonia (Westra and Choy 2009).

13.3.2 Ultrasound

The use of ultrasound as an imaging tool for pulmonary infections has been increasing especially for assessment of complications. Its utility is even more important because there is no associated radiation, no sedation, no specific preparation, and the ultrasound machine can be transported to the patient's bedside. It can be used for planning thoracentesis, thoracotomy, and image-guided drainage procedures. Lower-frequency (3.5–7 MHz) sector transducers are initially used for overview through inter- and subcostal scanning, but higher-frequency (10–12.5 MHz) linear transducers are helpful for more detail in the near field.

13.3.3 Computed Tomography (CT) Scan

The development of helical and multidetector CT has revolutionized imaging evaluation of pulmonary infections. The use of intravenous contrast medium also helps optimize the assessment of pleura, mediastinum, and pulmonary parenchyma in cases of complicated pneumonia. High-resolution CT (HRCT) shows greater accuracy in characterizing diseases into interstitial, airway, and airspace processes and gives a more accurate depiction of the extent of the disease. CT has an important role when a complication is suspected, to exclude an underlying abnormality in recurrent and persistent infections, for image-guided interventions, and for the evaluation of immunocompromised children (Westra and Choy 2009). Radiation-associated risks are important to consider, and thus, a clear indication for the procedure has to be present. Low radiation dose technique with 80–120 kVp, age and thoracic thickness-adjusted low milliampere-seconds, along with radiation dose modulation should be utilized.

13.3.4 Magnetic Resonance Imaging (MRI)

Evaluation of lung parenchyma with conventional MR imaging has limitations because of the inherent low proton density and weak MR signal as related to the low physical density of the lung. However, lung parenchymal, pleural, and lymph node inflammatory abnormalities can be visualized and characterized by MRI in children with pulmonary infections.

13.4 Specific Infections

13.4.1 Viral Infections

Peripheral airways disease or bronchiolitis are common terms ascribed to lower respiratory infection secondary to viruses. It commonly occurs in children less than 2 years of age, typically presenting with cough, coryza, and wheezing. RSV is the most common cause, but other viral causes include rhinovirus, parainfluenza virus, human metapneumovirus, adenovirus, influenza virus, coronavirus, and human bocavirus (Eslamy and Newman 2011). Following inhalation of infected aerosols, the virus migrates to small airways and alveoli resulting to bronchoconstriction and increased mucous secretion (Aherne et al. 1970; Swischuk and Hayden 1986).

Typical chest radiographic appearances are peribronchial thickening/opacities, hyperaeration, and subsegmental atelectasis (Fig. 13.1). The peribronchial inflammation and edema manifests as increased peribronchial cuffing or thickening of the bronchial walls, which is usually asymmetric and radiates from the hila into the lung. Narrowed distal airway lumen due to bronchiolar wall edema and mucus results in hyperinflation with areas of segmental and subsegmental atelectasis (Condon 1991; Donnelly 2001). Patchy areas of airspace consolidation have also been described in viral pneumonia. CT is rarely required in the investigation of viral lower respiratory infection, but the most common CT feature is peribronchial thickening and ground-glass attenuation without consolidation (Tanaka et al. 1996).

Varicella zoster virus infection is a highly contagious but a relatively benign, self-limited disease in childhood. Varicella pneumonia is regarded as a serious manifestation in adults, but immunocompromised children are also at risk. Clinically, cough, fever, dyspnea, chest pain, and vesicular rash are generally accompanied by mild constitutional symptoms (Kim et al. 1999). Radiographs of the chest initially reveal nodular infiltrates that may progress to large segmental areas of patchy consolidation, predominantly in the bases and perihilar regions. Total clearing is virtually guaranteed, although punctate calcifications maybe evident within 2 years after acute illness (Fig. 13.2). Airspace disease associated with chicken pox in children occurs most often in the immunocompromised host (Blickman 1998).

Certain groups of viruses have been recently reported to cause severe respiratory infection leading to respiratory failure and even death. The severe acute respiratory syndrome (SARS) caused by coronavirus A (SARS-CoV) created a scare in 2003 with over 8,000 cases reported from 29 different countries. SARS presents with a prodrome of flu-like illness, followed by cough, dyspnea, and possibly acute respiratory distress. The initial radiographic manifestation is the presence of focal or diffuse interstitial opacities but rapidly progresses to bilateral areas of consolidation (Thibodeau and Viera 2004) (Fig. 13.3). Another pandemic virus is the influenza virus A H5N1 (avian influenza virus), originating from Asia and spreading over many parts of the world from 2003 to 2007. More recently, influenza virus of swine origin, designated as influenza A H1N1, was first reported in Mexico

in 2009 and has rapidly spread globally. Symptoms range from asymptomatic infection to mild upper respiratory illness, viral syndrome, diarrhea, severe pneumonia, acute respiratory distress syndrome (ARDS), and progression to multiorgan failure. Initial chest radiographs in children with a mild and self-limited clinical course are often normal, but they may demonstrate prominent peribronchial markings with hyperinflation and multifocal areas of consolidation (Lee et al. 2010) (Fig. 13.4).

13.4.1.1 Complications of Viral Pneumonia

The most common complication of viral pneumonia is a secondary bacterial infection. Viral infection can compromise the respiratory mucosa and render the host pulmonary respiratory system susceptible to develop superimposed bacterial pneumonia (Donnelly 1999).

Postinfectious bronchiolitis obliterans (constrictive bronchiolitis or obliterative bronchiolitis) is a clinical syndrome of chronic airflow obstruction associated with inflammatory changes in the small airways as response to epithelial injury associated with infections. It is particularly associated with *Adenovirus*, RSV, *Varicella*, and severe *Mycoplasma* infection. The chest x-ray findings are often nonspecific and can appear normal, but the most common abnormality is hyperaeration (Yalcin et al. 2003). On HRCT, there is a mosaic perfusion pattern (Fig. 13.5). Perfusion is diminished in areas of parenchymal attenuation due to vasoconstriction secondary to hypoxia. Inspiratory and expiratory phases of ventilation are important in HRCT to better assess air trapping in this condition (Hansell et al. 1997). Peribronchial thickening, atelectasis, bronchiectasis, and sometimes lung volume reduction can also be seen. Swyer-James is a subtype of postinfectious bronchiolitis obliterans, which is typically unilateral. It can affect one lung segment, a lobe, or the entire lung. The characteristic chest radiographic and CT findings are hyperlucency due to the pulmonary hypoperfusion, reduction of vascular and hilar markings, and volume reduction of the affected lung or lobe (Daltro et al. 2011) (Fig. 13.6).

13.4.2 Bacterial Pneumonia

Bacterial pneumonia occurs with the inhalation of the infectious agent into the airspaces. It is most commonly caused by *S. pneumoniae*, *Haemophilus influenza* type B, and *Staphylococcus aureus*. *Staphylococcus* commonly occurs in early infancy, *Haemophilus* most often between 6 and 12 months, and *S. pneumoniae* more commonly between 1 and 3 years of age. Gram-negative aerobic bacteria such as *Pseudomonas aeruginosa* and *S. aureus* are a major problem in patients with cystic fibrosis. Patients present with cough, chest pain, and high fever.

Following inhalation of the infectious agent into the airspaces, acinar exudate and edema ensues, manifesting as localized airspace consolidation with air bronchogram on chest radiographs. The typical distribution is lobar or segmental, depending on the stage of progression at the time the x-ray was obtained (Fig. 13.7a) (Condon 1991; Donnelly 1999). Round pneumonia is a spherical pneumonia, usually caused by *S. pneumoniae* (Rose and Ward 1973) (Fig. 13.7b). It is common in children less than 8 years old, maybe due to poor development of collateral pathways of ventilation (pores of Kohn and channels of Lambert). When round pneumonia is seen in children over 8 years old, other etiologies should be considered. The CT manifestations of bacterial infection are areas of consolidation with or without air bronchogram, typically with a segmental or lobar distribution and involving the lung periphery (Tanaka et al. 1996).

13.4.2.1 Parapneumonic Effusions and Empyema

Parapneumonic effusions occur most commonly in bacterial pneumonia. It represents a spectrum of inflammatory fluid collections that ranges from transudative effusion to empyema. Parapneumonic effusions complicate pneumonia in 36–56 % of cases in pediatric patients (Kurt et al. 2006), and empyema complicates an estimated 0.6 % of all childhood pneumonias (Jaffe and Balfour-Lynn 2005).

Pleural fluid can usually be detected on a frontal chest radiograph, but layering of fluid on the lateral decubitus view distinguishes a free flowing fluid from a loculated fluid.

CT scan gives a better characterization of parapneumonic effusions compared to radiographs. CT findings include enhancement and thickening of the parietal and visceral pleura, thickening of the extrapleural subcostal tissues, and increased attenuation of the extrapleural subcostal fat (Muller 1993) (Fig. 13.8). These CT characteristics do not accurately predict empyema and should not be used to distinguish between empyema and transudative effusions. In ultrasound, pleural fluid can be characterized as simple effusion, complicated effusion, or fibrothorax (pleural thickening or fibrosis) (Fig. 13.9). A simple effusion appears as a clear anechoic or cloudy hypoechoic fluid with or without swirling particles. A complicated effusion appears as a septated or multiloculated, hypoechoic fluid with fibrinous septations, with no clear demarcation between the lung and pleural components, while a fibrothorax appears as a thickened, echogenic rind of pleural plaque (Kim et al. 2000).

13.4.2.2 Lung Complications of Bacterial Pneumonia

Suppurative lung parenchyma complications represent a spectrum of abnormalities including cavitary necrosis, lung abscess, pneumatocele, bronchopleural fistula, and pulmonary gangrene.

Necrotizing pneumonia or cavitary necrosis is a complication of severe lobar pneumonia, characterized by massive necrosis and liquefaction of lung tissues resulting to multiple cavities rather than a solitary one. It is most commonly caused by *S. pneumoniae* although *Aspergillus* and *Legionella* have also been implicated in the pediatric population (Hodina et al. 2002). Evidence of cavitary necrosis complicating pneumonia is often seen on CT before or in the absence of findings in chest radiography. CT findings include lung consolidation with decreased parenchymal enhancement, loss of lung-pleura margin, and multiple thin-walled cavities lacking an enhancing border. The adjacent visceral pleura is particularly fragile and tends to rupture, causing bronchopleural fistula (Hoffer et al. 1999) (Fig. 13.10). Cavitary necrosis indicates an intense and prolonged illness, but it usually resolves without surgical intervention (Donnelly and Klosterman 1997).

Lung abscesses are thick-walled cavities containing purulent material resulting from pulmonary infection. An air-fluid level with reactive rim is a typical imaging appearance, as compared to necrotizing pneumonia where cavities occasionally have air-fluid level but without rim of enhancement (Donnelly and Klosterman 1997) (Fig. 13.11). Differentiating the two is important because abscess not responding to therapy may require drainage, whereas necrotizing pneumonia does not require invasive treatment, and intervention may even be harmful resulting in complications such as bronchopleural fistula (Hoffer et al. 1999). Pneumatoceles are thin-walled cysts without septations that develop within the lung parenchyma after an acute pneumonia (Fig. 13.12). It may represent a later or less severe stage of resolving or healing necrosis and is most often associated with *S. aureus* (Daltro et al. 2011).

Bronchiectasis is the most common long-term sequelae of lung parenchymal damage from pneumonia. It is best demonstrated on high-resolution chest CT scan, and the main diagnostic features are as follows: internal diameter of the bronchus is wider than its adjacent pulmonary artery, failure of the bronchus to taper peripherally, and visualization of bronchi in the outer 1–2 cm of the lung zones (Eslamy and Newman 2011) (Fig. 13.13).

13.4.3 Pertussis

Pertussis is a highly contagious respiratory bacterial infection caused by *Bordetella pertussis*. It infects mainly infants and young children causing symptoms that include mild fever, runny nose, and cough, which develops into a paroxysmal cough followed by whooping (whooping cough). Pneumonia is a common complication, and untreated patients may be contagious for 3 weeks or more following onset of the cough. The spread of pertussis can be prevented by immunization.

Histopathologic examination reveals an infection dominated by necrotizing bronchiolitis, intra-alveolar hemorrhage, fibrinous edema, and angiolymphatic leukocytosis (Paddock et al. 2008). Conventional radiographs reveal streaky perihilar infiltrates with most often unilateral hilar adenopathy, a pattern sometimes called the shaggy heart appearance (Blickman 1998) (Fig. 13.14).

13.4.4 Mycoplasma Pneumonia

M. pneumoniae is a common ubiquitous organism and treatable cause of community-acquired pneumonia, occurring primarily in children and young adults. It accounts for up to 30 % of all pneumonia in the general population, but the highest incidence is seen in children between 3 and 14 years of age. Of those infected, 50 % get tracheobronchitis, 30 % pneumonia, 10 % pharyngitis, and 10 % otitis media. Clinically, symptoms are less severe but more common than in true bacterial pneumonia (Blickman 1998).

The radiographic findings are nonspecific, have a broad spectrum of appearances, and may present with a pattern intermediate between the classic viral and bacterial pneumonia patterns (Hsieh et al. 2007). Some authors reported that a reticulonodular pattern or nodular opacities are typical radiographic pattern (John et al. 2001), while others stress the occurrence of confluent and patchy consolidation (Reittner et al. 2000) (Fig. 13.15). HRCT findings are thickened bronchovascular bundles, ground-glass attenuation and consolidation, centrilobular nodules, and lobular distribution (Tanaka et al. 1996; Reittner et al. 2000).

13.4.5 Chlamydia Pneumonia

Chlamydia trachomatis is an obligate intracellular parasite. Genital chlamydial infection is recognized as the world's most common sexually transmitted disease, and the high prevalence in women of childbearing age results in exposure of neonates during childbirth. Chlamydia pneumonia is a neonatal infection acquired after passage of the fetus through the cervix and vagina. The infant typically presents at 3–6 weeks of age with respiratory symptoms and occasional pulmonary hemorrhage. *C. trachomatis* should be suspected in infants who are afebrile or nontoxic and have a dry cough. These patients often have a peripheral eosinophilic pleocytosis, sometimes with concomitant conjunctivitis (Ostapchuk et al. 2004). Most chest radiographs show bilateral hyperaeration and diffuse infiltrates with a variety of radiographic patterns including interstitial, reticular nodular, atelectasis, coalescence, and bronchopneumonia (Radkowski et al. 1981) (Fig. 13.16).

13.4.6 Tuberculosis

Tuberculosis (TB) is caused by infection with the *Mycobacterium tuberculosis* complex. Once inhaled, the infected aerosolized droplet in the alveoli cascades a series of inflammatory reaction, and the bacilli also spread to nearby mediastinal lymph nodes. The alveolar site of infection (Ghon focus), the infected lymph nodes, and the associated lymphangitis form the "primary (Ranke's) complex." In most immunocompetent children, the infection goes into latency and the bacilli become dormant. These children usually have a reactive tuberculin skin test (TST) and/or a positive Interforon-gamma release assay (IGRA) test, but without clinical evidence of TB and generally no abnormalities on chest radiograph apart from the primary complex residual. Primary tuberculosis disease occurs if the host is unable to contain the infection, and disease progression occurs in the lungs, the lymph nodes, and adjacent structures in the thorax or could disseminate in any part of the body.

Lymphadenopathy (present in 92 %) with or without a visible Ghon focus is the radiographic hallmark of TB infection and usually involves the hilar and paratracheal regions. The Ghon focus may be too small to be radiographically visible but can also undergo caseation and calcify (Fig. 13.17). Disease progression may occur at the site of Ghon focus, within the regional lymph nodes, or following disease spread (Fig. 13.18). Parenchymal involvement in primary pulmonary TB most commonly appears as homogeneous consolidation, although it can appear patchy, linear, nodular, and mass-like. Caseation necrosis, liquefaction, or calcifications can be seen within the consolidation and can progress into extensive lung damage (Marais et al. 2004) (Fig. 13.19). Enlarged and edematous hilar, paratracheal, and subcarinal lymph nodes may cause compression of the adjacent bronchus and can lead to hyperinflation or atelectasis of the affected lung segment. Contrast-enhanced CT shows a characteristic appearance consisting of central areas of low attenuation with peripheral rim enhancement and obliteration of perinodal fat (Kim et al. 1997) (Fig. 13.20).

Pulmonary dissemination, usually seen in very young and immunocompromised patients, leads to the formation of pulmonary nodular interstitial granulomas, usually 1–2 mm in size, throughout the lungs. Chest radiographs demonstrate the usual miliary nodular pattern but CT is more sensitive for the detection of miliary TB (Kim et al. 1997) (Fig. 13.21). Adult-type disease presentation is common after primary infection in children over 10 years of age or via endogenous reactivation (postprimary TB) or reinfection. Chest radiograph shows ill-defined, fibronodular parenchymal disease and cavitation mainly involving the apical segments of the upper lobes (Perez-Velez and Marais 2012) (Fig. 13.22).

13.4.7 Mycotic Infections

13.4.7.1 Aspergillosis

Aspergillus fumigatus is a ubiquitous saprophytic mold found in many environmental sites, and infection is usually via inhalation of spores, although other routes of entry also occur. Infection can manifest as colonization of airway cavities and necrotic tissue, allergic disease, and invasive disease, which is usually acute and rapidly progressive severe disease (Foster and Alton 2003).

Airway colonization occurs in patients with underlying airway disease such as asthma and bronchiectasis. Intertwined fungal hyphae, called as mycetoma or aspergilloma, form in the pulmonary cavity or ectatic bronchi. Important underlying causes are pulmonary TB with cavitation and cystic fibrosis with bronchiectasis. Rounded soft tissue mass within a cavity forming an "air-crescent" sign is a typical appearance (Fig. 13.23). Allergic bronchopulmonary aspergillosis is characterized by mucoid impaction of the proximal bronchi presenting as fingerlike shadows involving the upper lobes on the chest radiograph. CT demonstrates the mucoid impaction of the central airways and the bronchiectasis of the segmental or subsegmental airways (Foster and Alton 2003). Invasive disease is an aggressive, rapidly disseminating and destructive disease and occurs when host defenses are impaired. It is characterized by the occlusion of large- or medium-sized arteries by plugs of hyphae causing pulmonary hemorrhage, arterial thrombosis, and infarction. Radiographic findings are nonspecific, with multiple nodules or areas of consolidation (Fig. 13.24). The typical CT finding is the halo sign due to ground-glass attenuation representing hemorrhage surrounding the pulmonary nodule or mass (Foster and Alton 2003; Eslamy and Newman 2011).

13.4.7.2 Histoplasmosis

Histoplasmosis, caused by the fungus *Histoplasma capsulatum*, is usually an asymptomatic and self-limited disease that rarely requires therapy in children other than the very young or immunocompromised. It is found in the soil of endemic areas including Central United States, Central America, and Northern South America but has also been reported in some parts of Asia (Houston 1994). After inhalation, the spores germinate within the alveoli inciting an intense tissue reaction characterized by granulomas, which may calcify. It spreads to the lymphatics and into the hilar or mediastinal lymph nodes, and systemic dissemination may occur in patients with impaired T-cell immunity (McAdams et al. 1995).

Histoplasmosis falls in one of three categories: acute, chronic pulmonary, and disseminated disease. Acute pulmonary histoplasmosis is a self-limited illness. Chronic pulmonary histoplasmosis occurs in patients with chronic lung

disease and presents similar to tuberculosis with predilection for apical and posterior segments of the lung. Disseminated histoplasmosis in children is characteristically a fulminant illness, which may or may not have pulmonary involvement. Radiologic manifestations parallel the clinical syndromes. Acute disease usually manifests as focal parenchymal consolidation with or without ipsilateral hilar adenopathy (Fig. 13.25). With healing, a nodule representing a histoplasmoma may result. Chronic histoplasmosis radiographically manifests as an upper lobe fibrocavitary disease indistinguishable from postprimary tuberculosis. Chest radiographs of patients with disseminated disease may show miliary or diffuse reticulonodular pattern that could progress to diffuse airspace opacification (McAdams et al. 1995).

13.4.8 Parasite Infections

13.4.8.1 Echinococcosis

Echinococcosis, also known as hydatid disease or hydatidosis, is a parasitic infection in humans caused by dog tapeworm, *Echinococcus granulosus*, in its larval stage. It is endemic in many sheep and cattle-raising countries throughout the world. Humans are intermediate hosts and become infected through ingestion of contaminated water or vegetables. When eggs of adult tapeworm are ingested, embryos are freed and migrate through the host's gastrointestinal mucosa and enter the portal vein and lymphatic system to various parts of the body where the embryo develops into a cyst. The wall of the cysts contains three layers: the outermost, pericyst; the middle laminated membrane layer, ectocyst; and innermost germinal layer, endocyst (Czermak et al. 2001). The lungs are the most common sites of infection in children but majority remain asymptomatic until the cyst enlarges to cause symptoms due to mass effect or due to cyst rupture (Santivanez and Garcia 2010).

Diagnosis is obtained by imaging evaluation, supported by serology. A high proportion of lung lesions are discovered incidentally on a routine x-ray, and the most prominent radiological finding is a dense, round, well-demarcated opacity that can resemble a neoplasm (Fig. 13.26a). When the growth of the cyst produces erosion in the bronchioles, air between the endocyst and pericyst can produce a "crescent or inverse crescent sign." If air continues to enter the cyst cavity, endocyst membrane can be seen floating in the most dependent part of the pericyst cavity producing the "water-lily sign" (Fig. 13.26b). CT recognizes the appearance of the cystic lesion including smaller cysts, assesses signs of cyst rupture, evaluates the surrounding structures, and helps exclude alternative differential diagnoses (Santivanez and Garcia 2010).

13.4.8.2 Ascariasis and Hookworms

Ascariasis and hookworms remain the most common intestinal nematodes in the world (Sarinas and Chitkara 1997). In the western hemisphere, parasitic pneumonia secondary to *Toxoplasma gondii* is associated with compromised hosts, particularly acquired immunodeficiency syndrome (AIDS) patients. *Strongyloides stercoralis* infestation is seen in patients receiving glucocorticoids or chemotherapy and in patients with AIDS or other causes of T-cell dysfunction (Berk and Verghese 1998). *Ascaris* infestation generally occurs through hand-to-mouth ingestion of food contaminated with parasite eggs, while hookworms are transmitted through larval penetration of the skin. Symptomatic pulmonary disease may present with fever, cough, chest pain, hemoptysis, dyspnea, and wheezing. These pulmonary symptoms could be due to Loffler's syndrome, effects of larval tissue migration, airway reactivity or bronchospasm, superimposed bacterial infection, and chronic eosinophilic pneumonia (Sarinas and Chitkara 1997). *Ascaris* and hookworm infections present with peripheral eosinophilia during larval migration phase. Chest radiographs could be normal or demonstrate nonspecific patchy pulmonary infiltrates (Fig. 13.27). CT scan could depict abnormalities better and could show ground-glass pulmonary lesions with ill-defined margins as well as nodules (Sakai et al. 2006).

13.4.9 Pulmonary Infections in the Immunocompromised Children

Causes of immunodeficiency can be divided into congenital (primary) and acquired (secondary). The range of respiratory complications encountered is broad and is influenced by both the type and degree of immunodeficiency. Chest radiographs are insensitive and may show only subtle change. HRCT detects abnormalities not visible on the plain film such as bronchial wall thickening, bronchial dilatation, and air trapping.

Various noninfectious pulmonary processes including alveolar hemorrhage, pulmonary edema, graft versus host disease, and drug reaction are also seen in the immunocompromised hosts, which can mimic pulmonary infection on imaging.

13.4.9.1 Primary Immunodeficiency

The primary or congenital immunodeficiency disorders are inherited group of disorders resulting from innate defects of the immune system. Clinical manifestations are diverse and nonspecific, which include recurrent infections, infection with opportunistic organisms, failure to thrive, skin rashes, recurrent skin sepsis, and unusual wound healing (Jeanes and Owens 2002). Primary immunodeficiency can be broadly

divided into T-cell (cellular) immune deficiency versus B cell (humoral deficiency). Humoral immunodeficiencies are the most commonly encountered type characterized by defective antibody production with increased susceptibility to pyogenic infections but able to recover from viral infections (Fig. 13.28). Examples are X-linked agammaglobulinemia, IgA deficiency, and common variable immunodeficiency. Cellular immunodeficiencies have increased susceptibility to disseminated viral and opportunistic infections. Cellular immune disorders include DiGeorge syndrome and severe combined immunodeficiency (Collingsworth 2005).

13.4.9.2 Secondary Immunodeficiency

Acquired immunodeficiencies in childhood can be caused by chemotherapy, radiation therapy, immunosuppressive therapy aimed at treating childhood malignancies, transplant rejection, rheumatologic disorders, or inflammatory or infectious diseases. It can also be due to human immunodeficiency virus (HIV) infection, malnutrition, or any state of chronic debilitation.

Bone marrow transplant requires complete eradication of the immune system. Early infectious complications are frequently caused by bacteria and fungi, most commonly Gram-negative bacteria (*Pseudomonas* and *Klebsiella*) and *Aspergillus* (Fig. 13.29). Widespread use of long-term indwelling catheters has led to an increased incidence of both staphylococcal and streptococcal pneumonia. Chest radiographs may show classic focal or lobar consolidation although atypical appearance can also be seen. Children are also at increased risk of viral infections, most importantly RSV, *Herpes simplex*, *Adenovirus*, and *Varicella*. Immunosuppressive therapy following solid organ transplantation predisposes a patient to recurrent pulmonary infections. In these patients, viral infections can be life-threatening, but *Pneumocystis* and fungal infections (*Aspergillus* and *Candida*) can also be seen (Collingsworth 2005).

13.4.9.2.1 HIV/AIDS

Children represent 2 % of the reported cases of human immunodeficiency virus (HIV) infection. Most children are infected after vertical transmission from their mother, and majority develop acquired immunodeficiency syndrome (AIDS) early in life. There is increased susceptibility to bacterial, viral, fungal, protozoal, and opportunistic infections. Lobar or segmental consolidations are the most common patterns (Marks et al. 1996). Mycobacterial infection can be seen in AIDS patients, and the radiographic appearance mimics that seen in immunocompetent children with primary tuberculosis. *Mycobacterium avium-intracellulare* is also encountered later in the course of disease and imaging findings cannot be distinguished with other forms of mycobacterial infections (Collingsworth 2005). *Pneumocystis jiroveci* is the most common opportunistic pulmonary infection in children with AIDS, occurring in up to 50 %, and is the leading pulmonary cause of death (Jeanes and Owens 2002). Radiographic appearances are variable and include hyperinflation with diffuse bilateral interstitial or nodular infiltrates from the perihilar region to the periphery, which often progresses to widespread alveolar opacities with air bronchogram (Fig. 13.30). Cavitary nodules and cysts can be seen, with pneumothorax and/or pneumomediastinum as common complications. HRCT findings include patchy or diffuse ground-glass opacity, consolidation, cyst or cavities, centrilobular opacities, nodules, peribronchial cuffing, and interlobular septal thickening (Jeanes and Owens 2002; Collingsworth 2005).

13.5   Illustrations: Infections

13.5.1 Respiratory Syncytial Virus (RSV) Infection
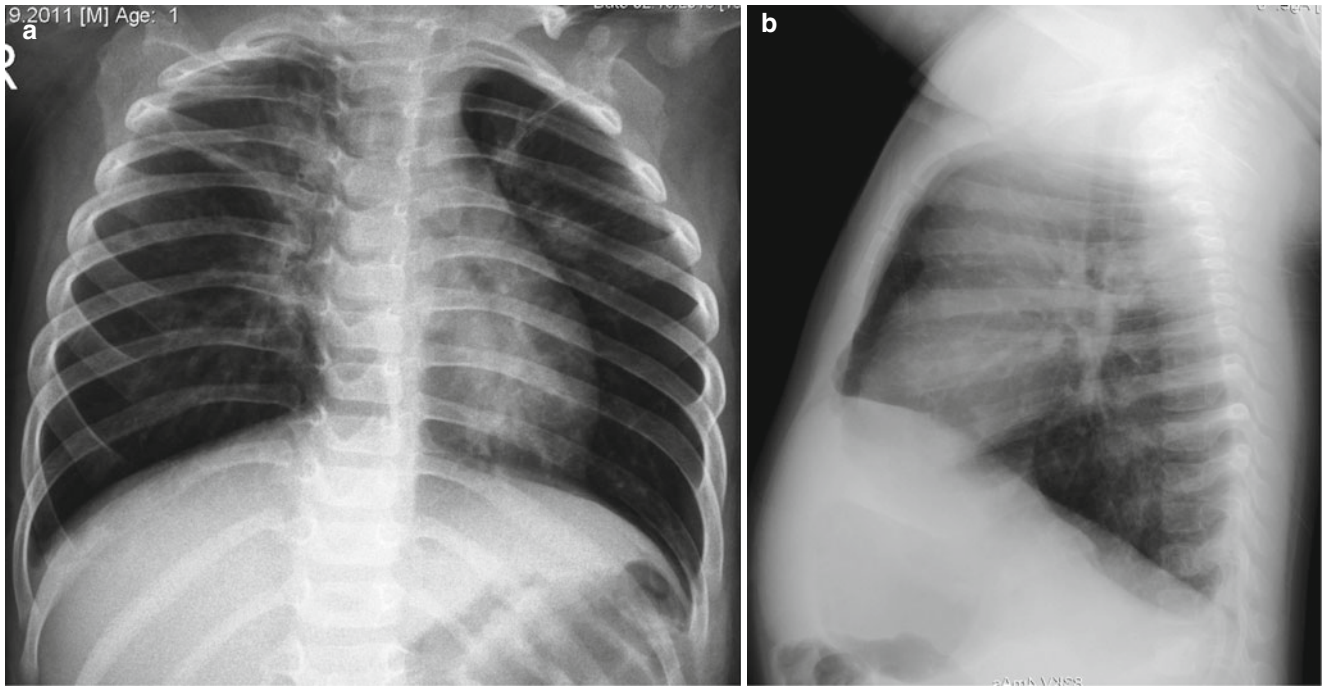
Fig. 13.1 Respiratory syncytial virus (RSV) infection in an 18-month-old boy. Frontal (**a**) radiograph demonstrates hyperaeration, perihilar peribronchial thickening, and areas of subsegmental atelectasis. Lateral view (**b**) shows depression of the diaphragm compatible with hyperaeration

13.5.2 Varicella Pneumonia
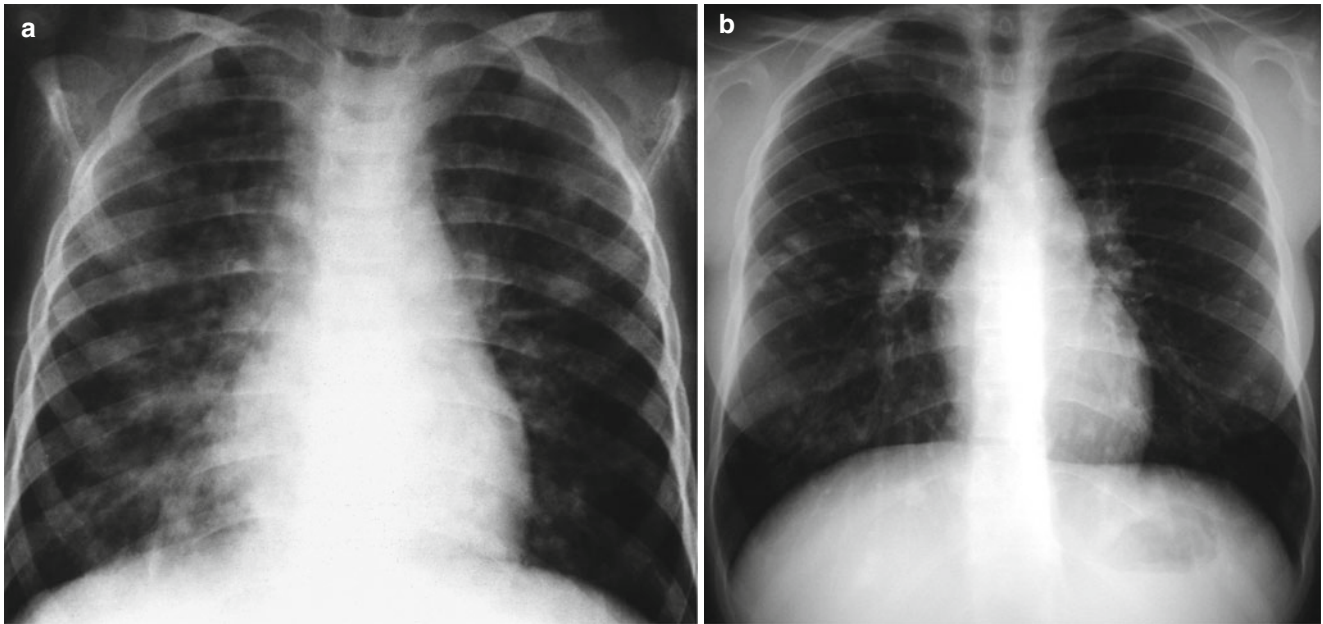
Fig. 13.2 Varicella pneumonia. Frontal chest radiograph of a 5-year-old boy showing multifocal patchy, nodular infiltrates throughout both lung fields (**a**). School requirement chest x-ray of a 15-year-old asymptomatic girl shows multiple, small, calcified nodules in both lung fields. The patient had varicella pneumonia 3 years prior (**b**)

13.5.3 SARS Infection
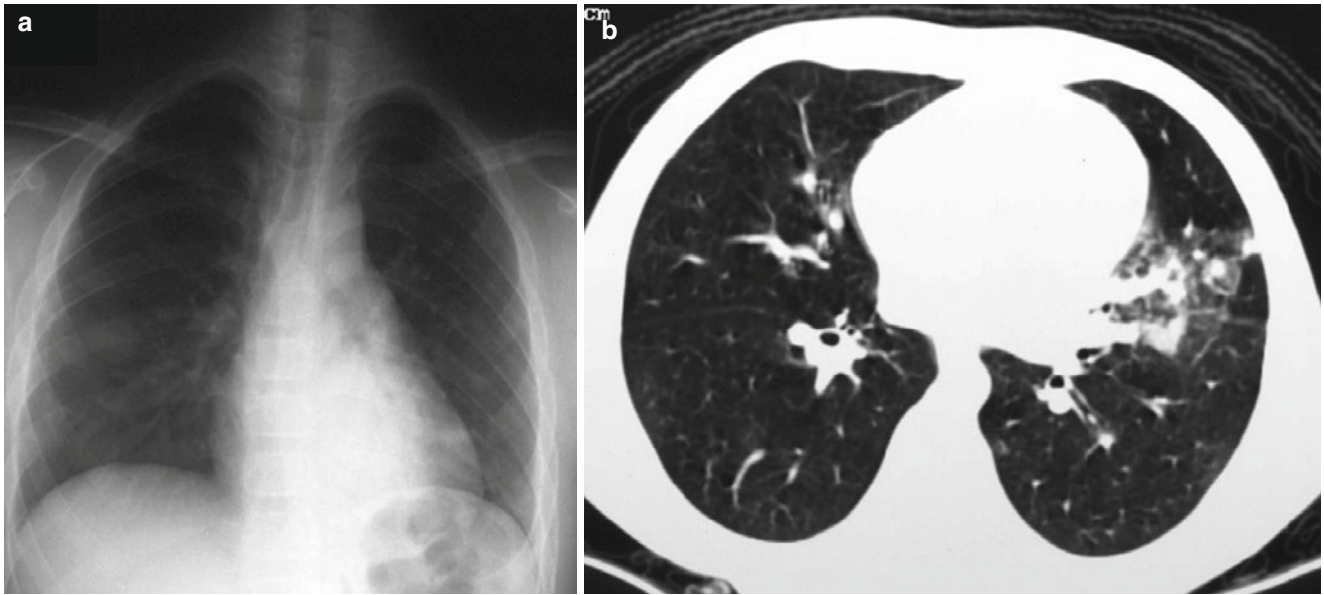
Fig. 13.3 SARS infection. Chest radiograph of a 13-year-old boy 3 days after the onset of fever shows ill-defined haziness in bilateral lower zones (**a**). An 8-year-old boy with confirmed SARS shows an area of mixed ground-glass opacity with consolidation in the lingula on HRCT (**b**) (Cases courtesy of Winnie CW Chu, MD, from Hong Kong)

13.5.4 Influenza AH1N1 Virus Pneumonia
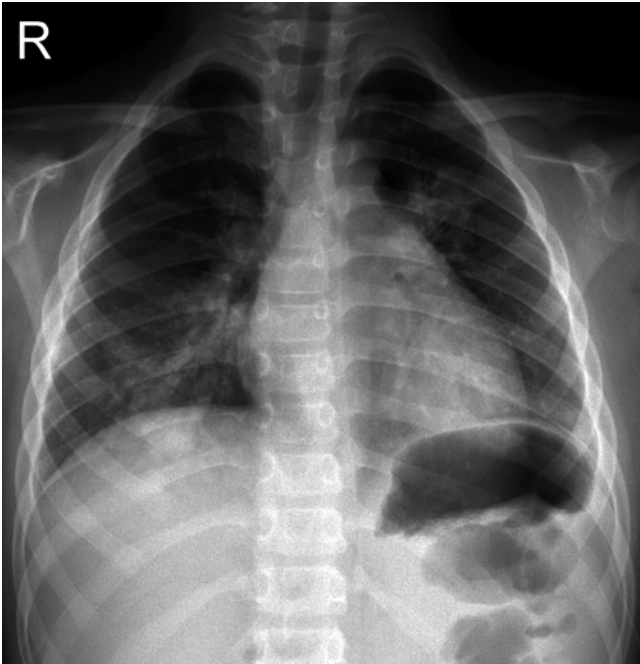
Fig. 13.4 AH1N1 virus pneumonia. Frontal chest radiograph shows generalized increase interstitial markings with multifocal patchy infiltrates (Case courtesy of Xanthe Marie Javier MD, from Philippines)

13.5.5 Postinfectious Bronchiolitis Obliterans

Fig. 13.5 Postinfectious bronchiolitis obliterans. High-resolution CT scan images in expiratory phase demonstrate the typical "mosaic perfusion" pattern

13.5.6 Swyer-James Syndrome
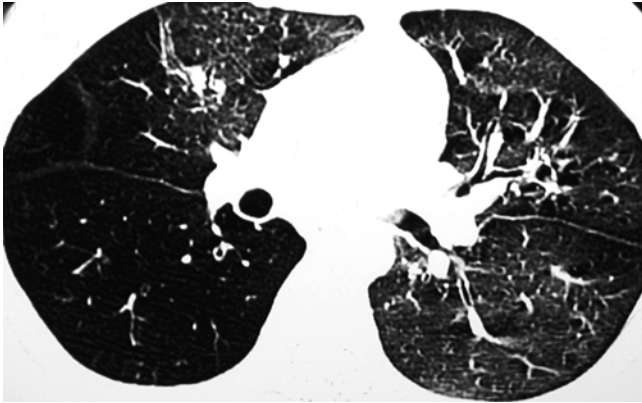
Fig. 13.6 Swyer-James syndrome in a 10-year-old girl. HRCT shows reduced attenuation and paucity of bronchovascular markings in the right lung (Case courtesy of Winnie CW Chu, MD, from Hong Kong)

13.5.7 Bacterial Pneumonia
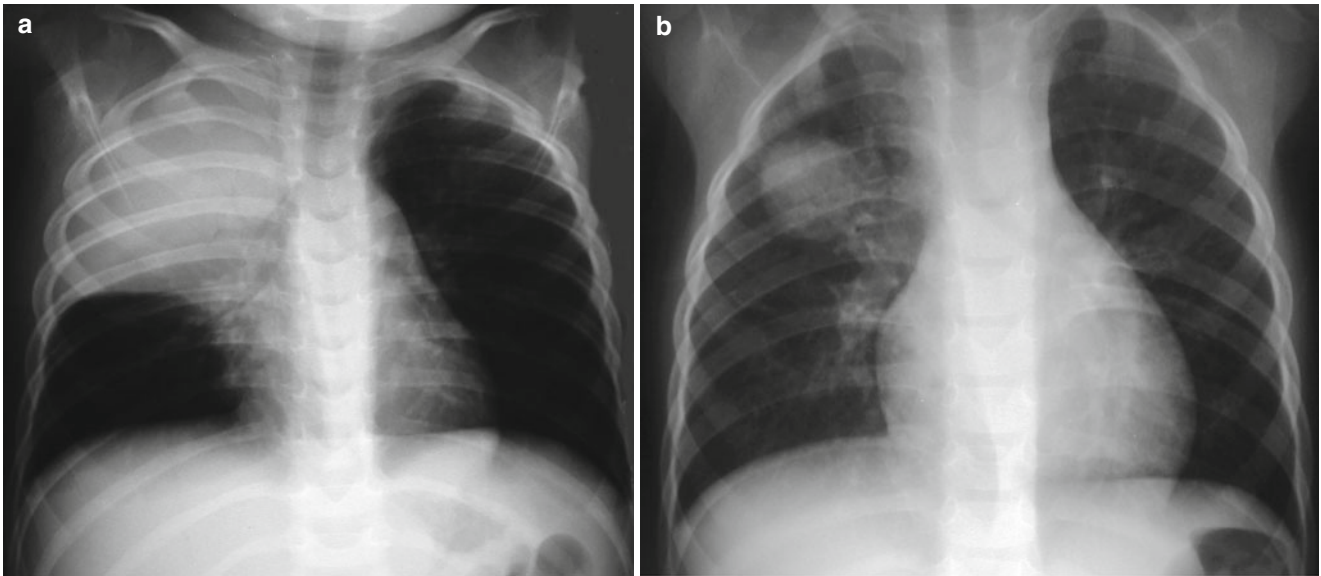
Fig. 13.7 Bacterial pneumonia. Chest radiographs of a 3-year-old girl with high fever, cough, and leukocytosis (**a**) demonstrate complete opacification of the right upper lobe. Image (**b**) shows a round, mass-like consolidation compatible with round pneumonia

13.5.8 Parapneumonic Fluid Collection: CT Finding
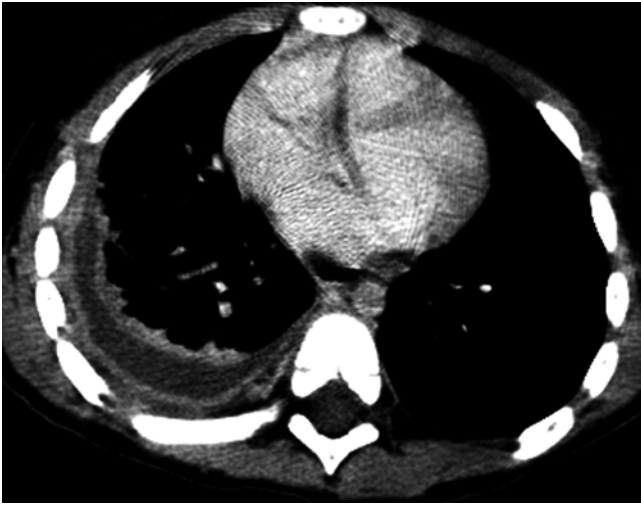
Fig. 13.8 Parapneumonic fluid collection on CT scan. Image demonstrates right-sided pleural fluid with thick enhancement of both visceral and parietal pleura

13.5.9 Parapneumonic Fluid Collection: Ultrasound Finding
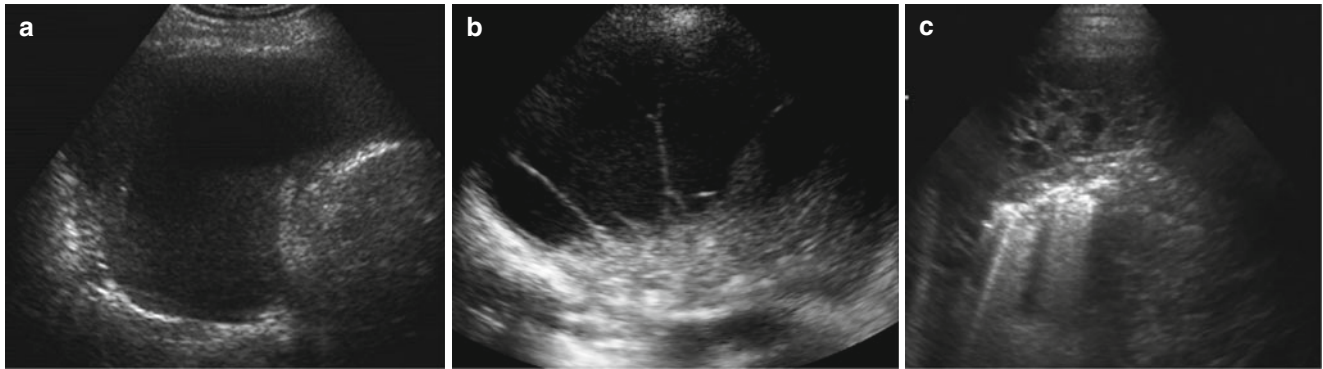
Fig. 13.9 Parapneumonic fluid collections on ultrasound. Simple effusion showing anechoic fluid without septations (**a**). Complicated fluid collection with thin septations and proteinaceous debris (**b**). Multiloculated fluid collection with thick septations and thickened pleural lining, compatible with fibrothorax (**c**)

13.5.10 Necrotizing Pneumonia
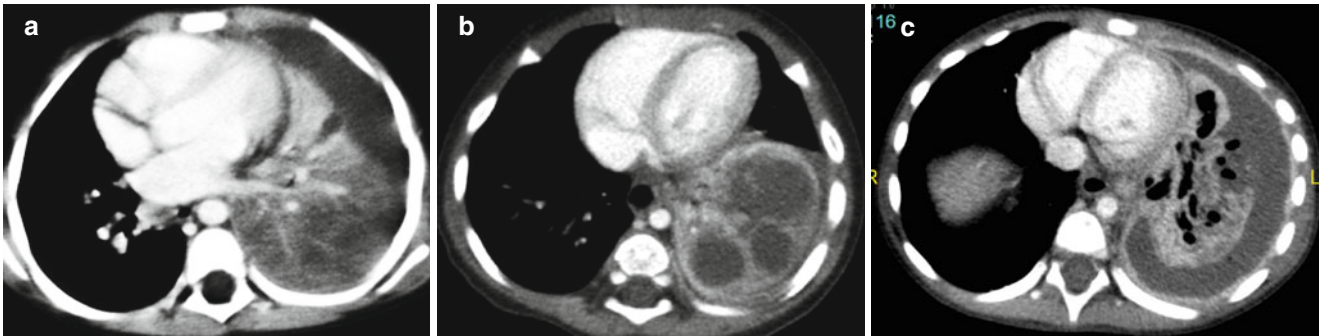
Fig. 13.10 Necrotizing pneumonia on CT. Left lower lobe consolidation showing diminished perfusion at the posterior region (**a**). Evolution of lung ischemia with development of multiple fluid-filled cavities (**b**). Cavitary necrosis of the consolidation with bronchopleural fistula and parapneumonic fluid (**c**)

13.5.11 Lung Abscess

Fig. 13.11 Lung abscess. Chest radiograph of a 7-year-old boy with cough and high fever reveals a large abscess with air–fluid level and thick irregular border in the right mid-lung. Notice other smaller abscess inferior to the primary lesion

13.5.12 Pneumatocele
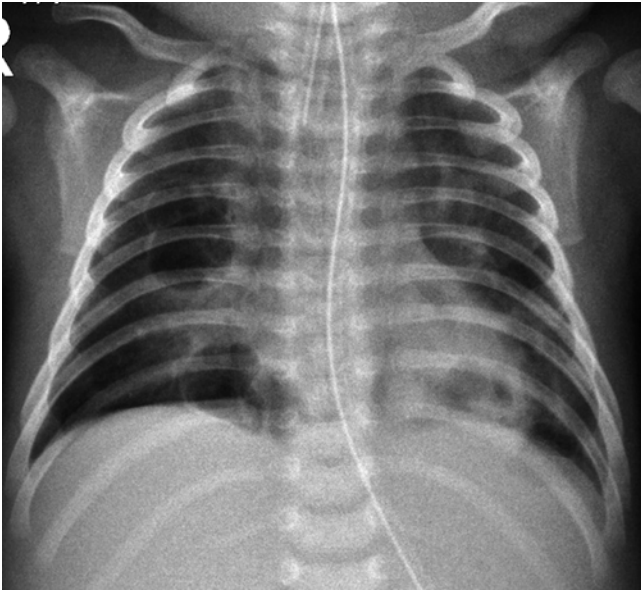
Fig. 13.12 Pneumatocele. A 6-month-old boy recovering from *Staphylococcus* pneumonia reveals thin-walled cysts in the right mid-lung field and bibasilar regions

13.5.13 Bronchiectasis
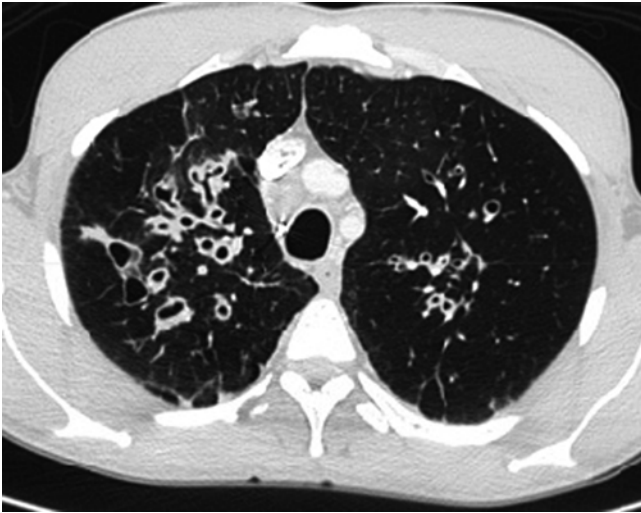
Fig. 13.13 Bronchiectasis. Axial HRCT image showing thick-walled, dilated bronchi with diameters wider than the adjacent pulmonary arteries

13.5.14 Pertussis

Fig. 13.14 Pertussis. Chest radiograph of an 18-month-old boy showing right hilar adenopathy with streaky perihilar infiltrates obscuring the cardiac shadow (shaggy heart) (Case courtesy of Marion O. Sanchez, MD, from Manila, Philippines)

13.5.15 Mycoplasma Pneumonia
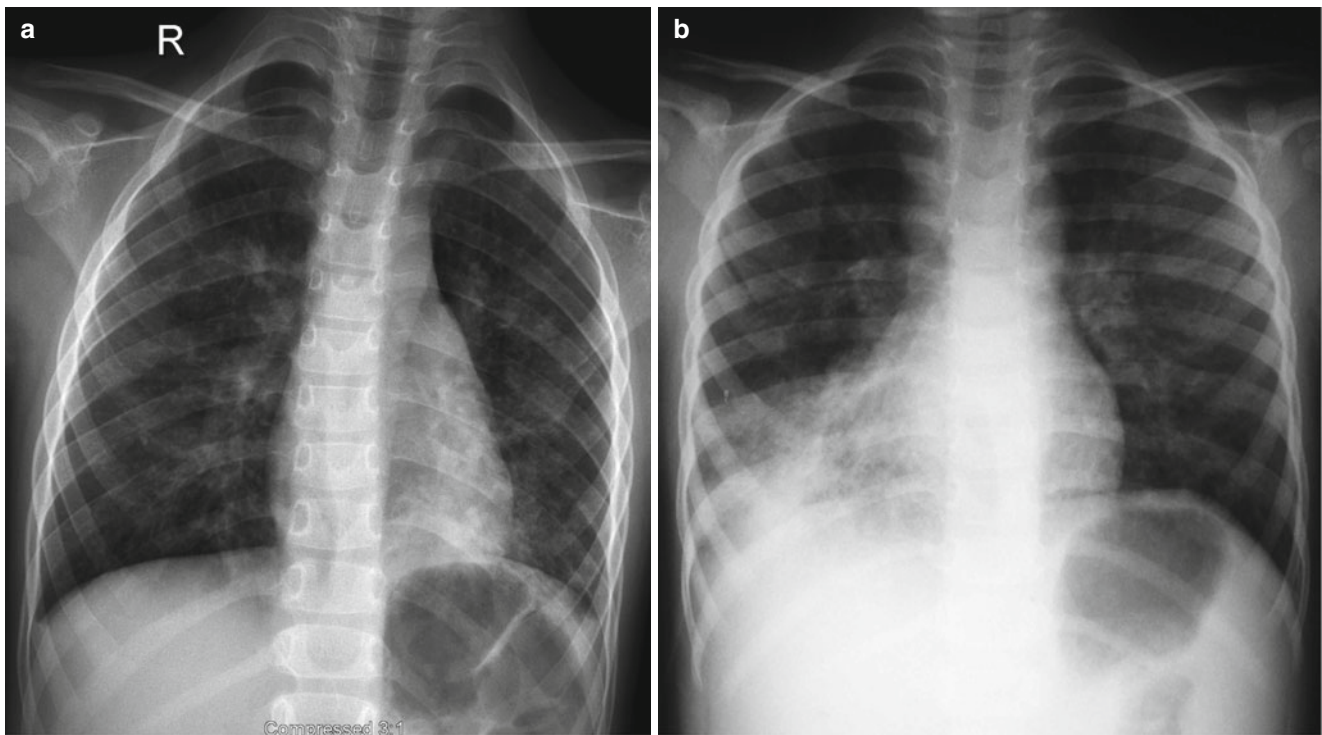
Fig. 13.15 Variable imaging pattern of Mycoplasma pneumonia. Chest x-ray of a 10-year-old boy (**a**) demonstrates generalized increase interstitial marking with scattered patchy areas of opacity. Another patient diagnosed with Mycoplasma infection demonstrating patchy consolidation on the right middle and lower lobes (**b**)

13.5.16 Chlamydia Pneumonia
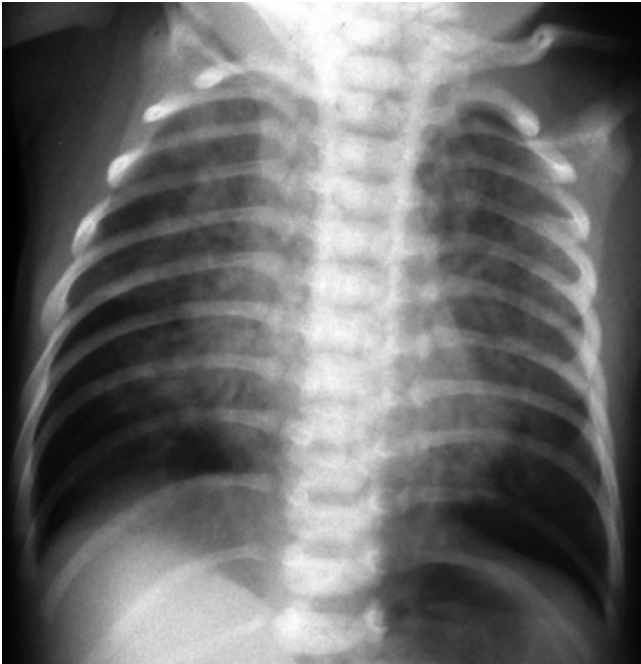
Fig. 13.16 Chlamydia pneumonia. Radiograph of an afebrile 2-week-old girl with dry cough shows bilateral hyperaeration and diffuse interstitial infiltrates, appearing coalescent on the right

13.5.17 Tuberculosis: Primary TB
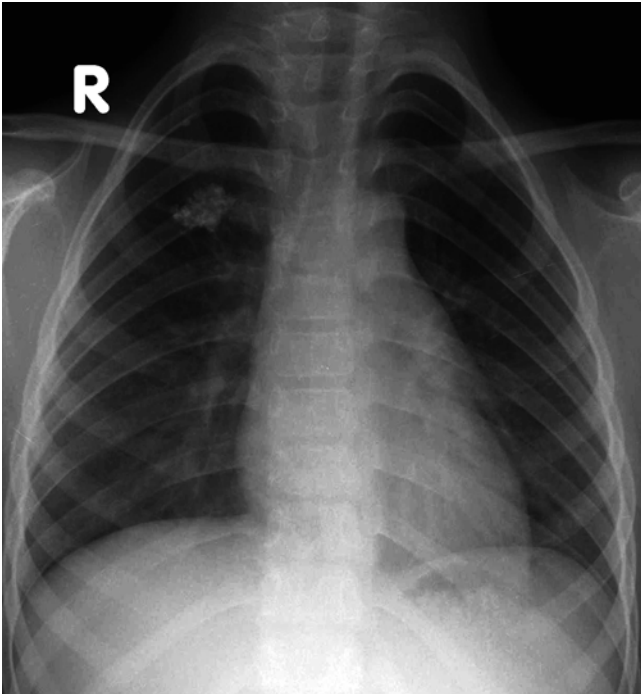
Fig. 13.17 Primary TB infection. An asymptomatic 7-year-old boy had a chest x-ray as a school requirement, which reveals a calcified granuloma on the right upper lobe. This corresponds to a calcified Ghon focus, a sign of TB infection

13.5.18 Tuberculosis: Primary TB
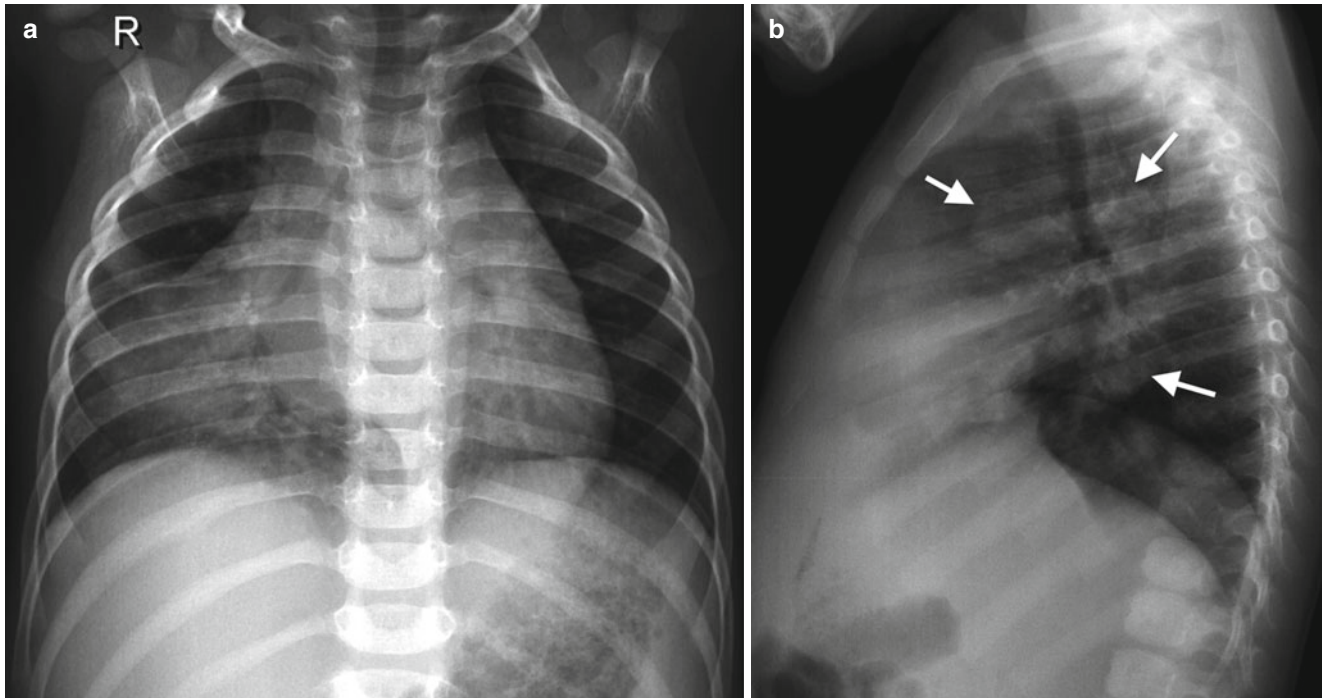
Fig. 13.18 Primary TB disease. Chest radiographs of a 2-year-old girl with chronic cough and fever showing dense right middle lobe consolidation on the frontal view (**a**) and extensive lymphadenopathy (*white arrows*) on the lateral view (**b**)

13.5.19 Tuberculosis: Progression of Ghon Focus
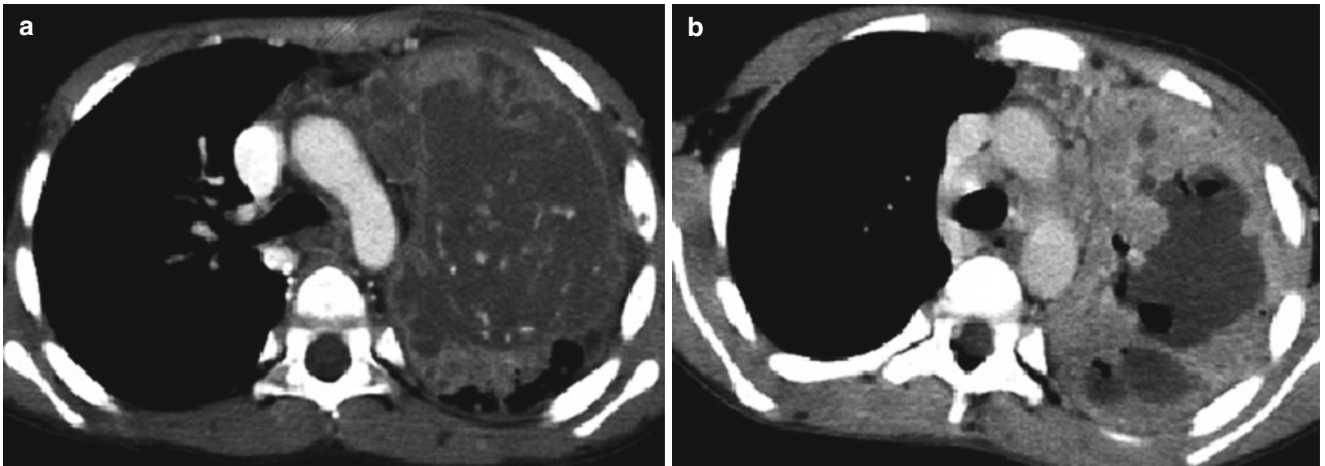
Fig. 13.19 Progression of Ghon focus. CT scan images from two different patients showing advanced progression of lung parenchymal disease from dense consolidation with ischemic changes (**a**) and cavitary necrosis with cyst formation (**b**)

13.5.20 Tuberculosis: Progression of Lymph Node Disease
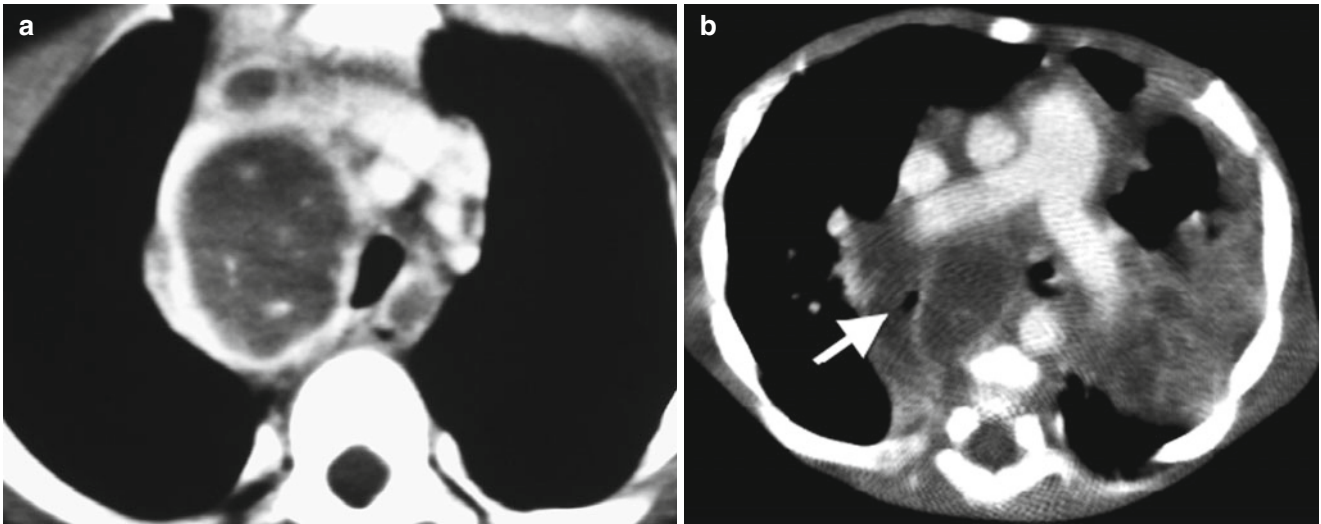
Fig. 13.20 Progression of lymph node disease. Image (**a**) demonstrates an enlarged right paratracheal lymph node effacing the trachea, with central hypoattenuation and peripheral contrast enhancement. Image (**b**) shows extensive subcarinal lymph nodes effacing the bronchi, especially the right mainstem bronchus (*white arrow*)

13.5.21 Miliary TB
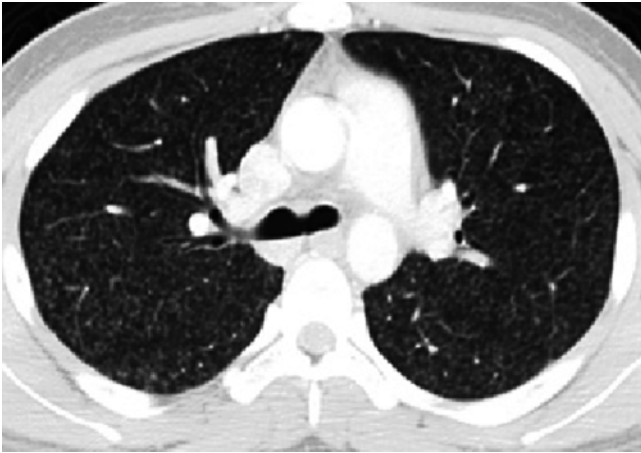
Fig. 13.21 Miliary TB. Axial CT image showing small (1–2 mm), uniform nodular densities scattered throughout both lungs compatible with disseminated TB disease

13.5.22 Reactivated TB
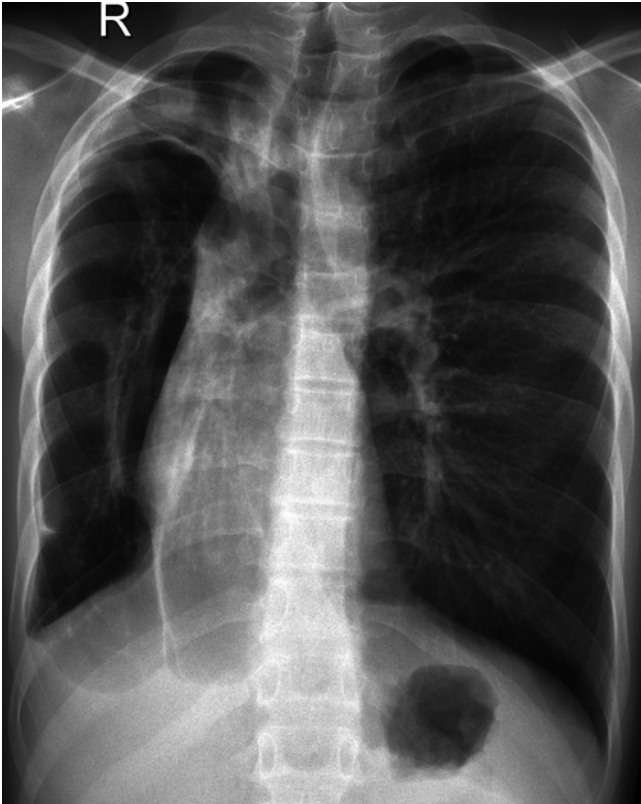
Fig. 13.22 Reactivation TB. Chest radiograph of a 13-year-old boy with chronic cough and shortness of breath showing fibrotic changes, pleural thickening, and volume loss in the right lung
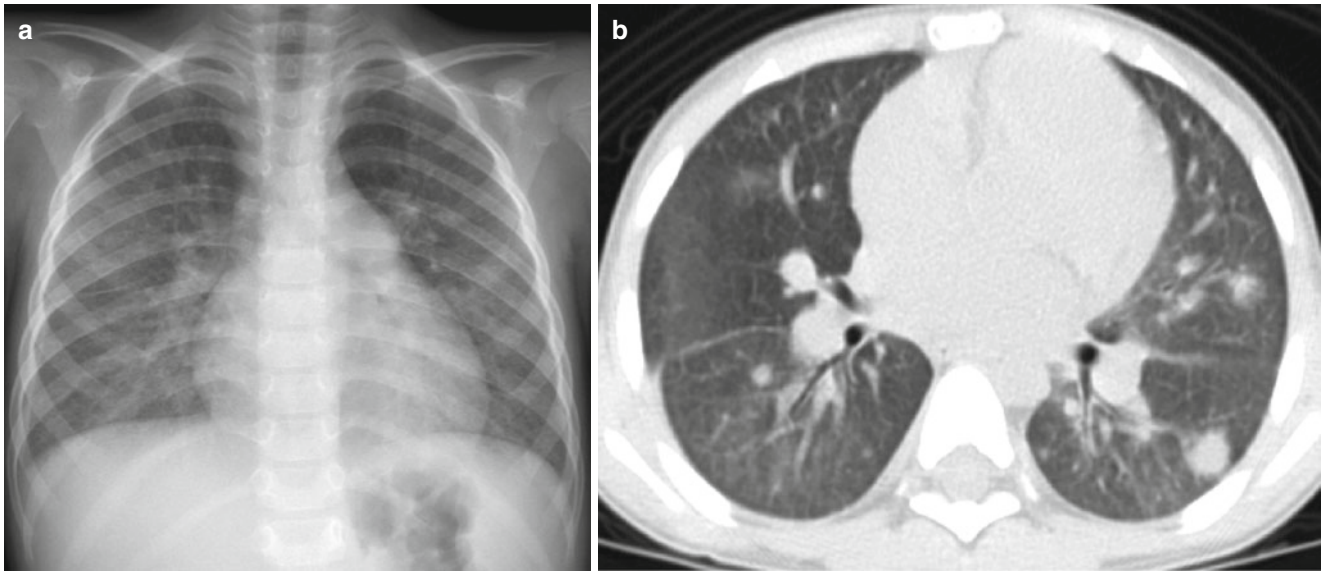
13.5.23 Aspergilloma

Fig. 13.23 Aspergilloma. Axial CT image of a 17-year-old girl with a soft tissue mass (aspergilloma) within a cavity in the left upper lobe, forming the "air-crescent sign"

13.5.24 Invasive Aspergillosis

Fig. 13.24 A 5-year-old boy with confirmed invasive aspergillosis disease. Chest radiograph (**a**) is nonspecific but suspected nodules are seen on the left lung. Axial CT image (**b**) confirms the presence of non-calcified pulmonary modules in both lungs

13.5.25 Histoplasmosis
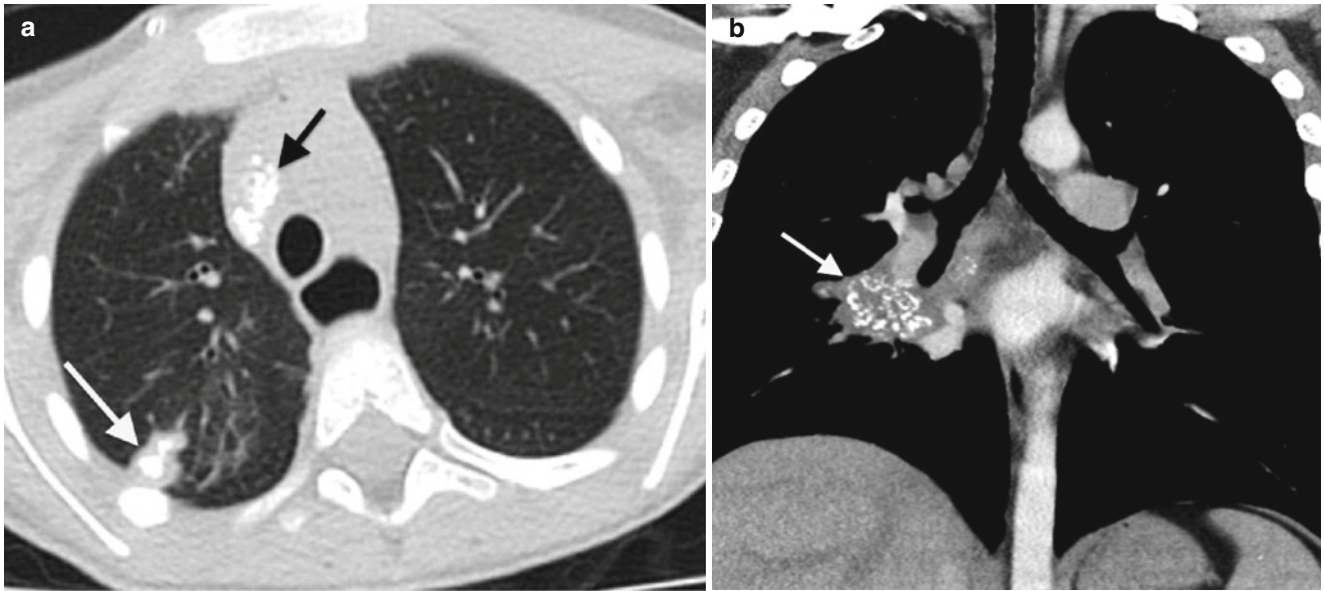
Fig. 13.25 Histoplasmosis in two different patients. Axial CT image of a 4-year-old boy (**a**) showing a calcified pulmonary nodule in the right upper lobe (*white arrow*) and calcified lymph nodes in the pretracheal region (*black arrow*). Coronal reconstructed CT image on a 7-year-old girl (**b**) shows a confluence of lymph nodes in the right infrahilar region with calcifications (*white arrow*) (Cases courtesy of Beth Kline-Fath, MD, from Cincinnati, Ohio, USA)

13.5.26 Hydatid Disease
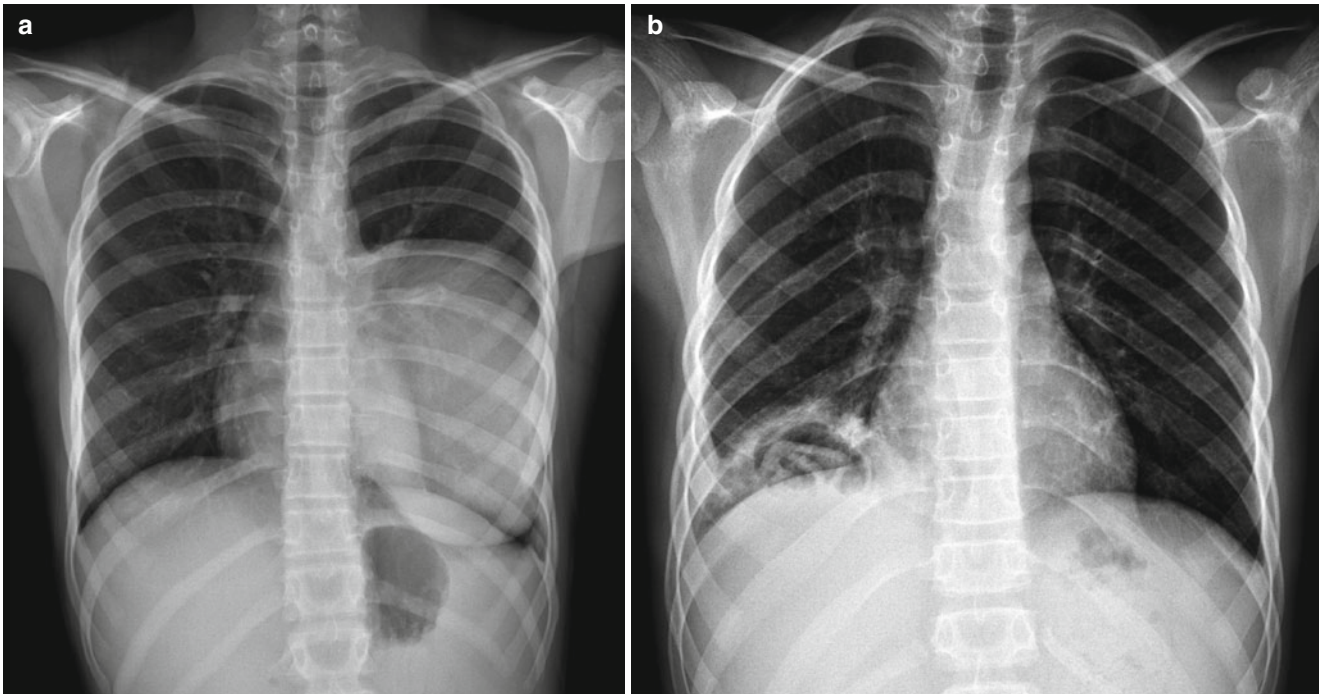
Fig. 13.26 Hydatid disease. (**a**) Radiograph of a 13-year-old girl who presented with cough and chest pain shows a mass-like opacity in the left lower lobe, later confirmed to be Echinococcus infection. (**b**) A 12-year-old boy with abdominal pain had a chest x-ray showing curvilinear opacities within a cyst in the right lower lobe. This is compatible with the "water-lily" sign in hydatidosis (Cases courtesy of Ali Yikilmaz, MD, from Turkey)

13.5.27 Ascariasis
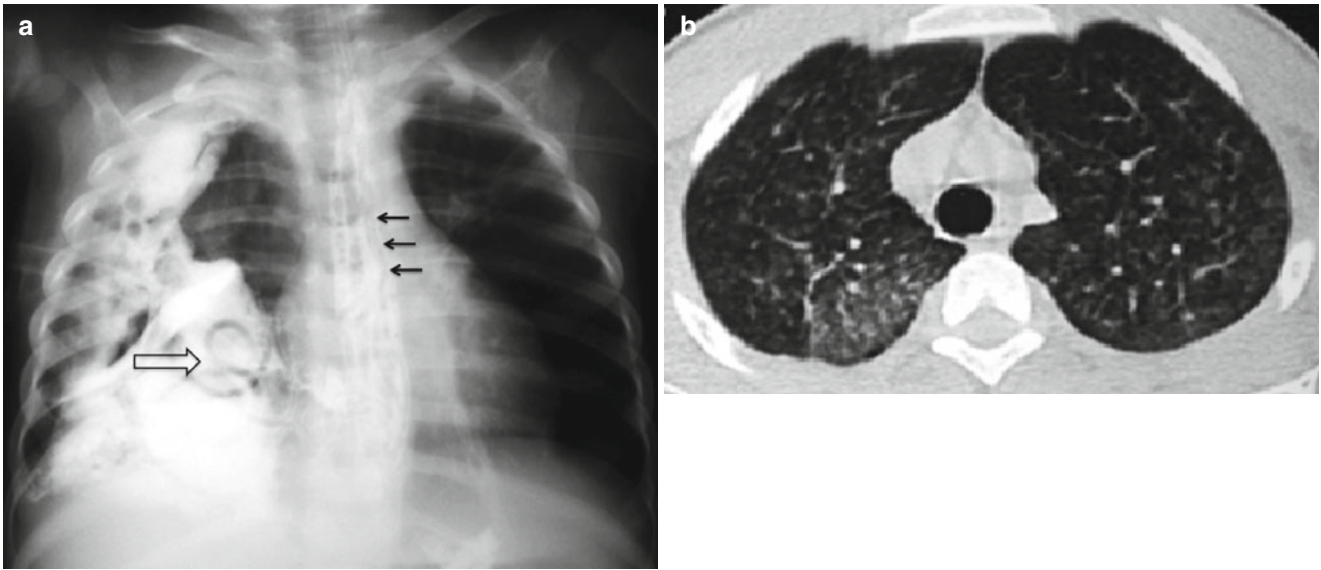
Fig. 13.27 Ascariasis. Chest radiograph following barium study (**a**) demonstrates *Ascaris* within the esophagus (*small black arrows*) as well as in the right pleural cavity (*open arrow*) indicative of esophageal perforation. Image (**a**) is an axial CT scan image from a patient with fever, peripheral eosinophilia, and stool samples with *Ascaris* eggs (Cases courtesy of Edson Marchiori, MD, from Rio de Janeiro, Brazil)

## 13.5.28 Staphylococcal Abscess
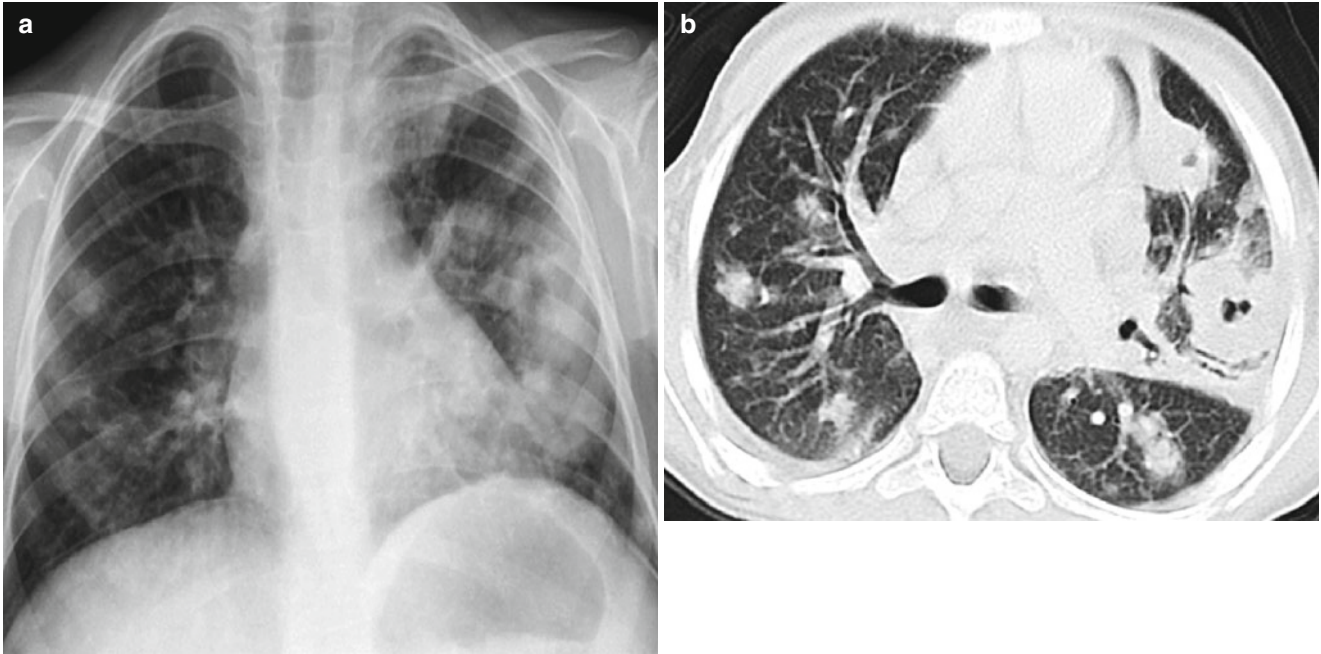
Fig. 13.28 Staphylococcal abscess. A 9-year-old boy with chronic granulomatous disease with persistent fever had a chest x-ray (**a**) showing multiple rounded opacities in both lung fields. Axial CT scan (**b**) demonstrates multiple pulmonary nodules, some on the left has cavitation. These are proven to be multiple abscesses

13.5.29 Aspergillosis in the Immunocompromised
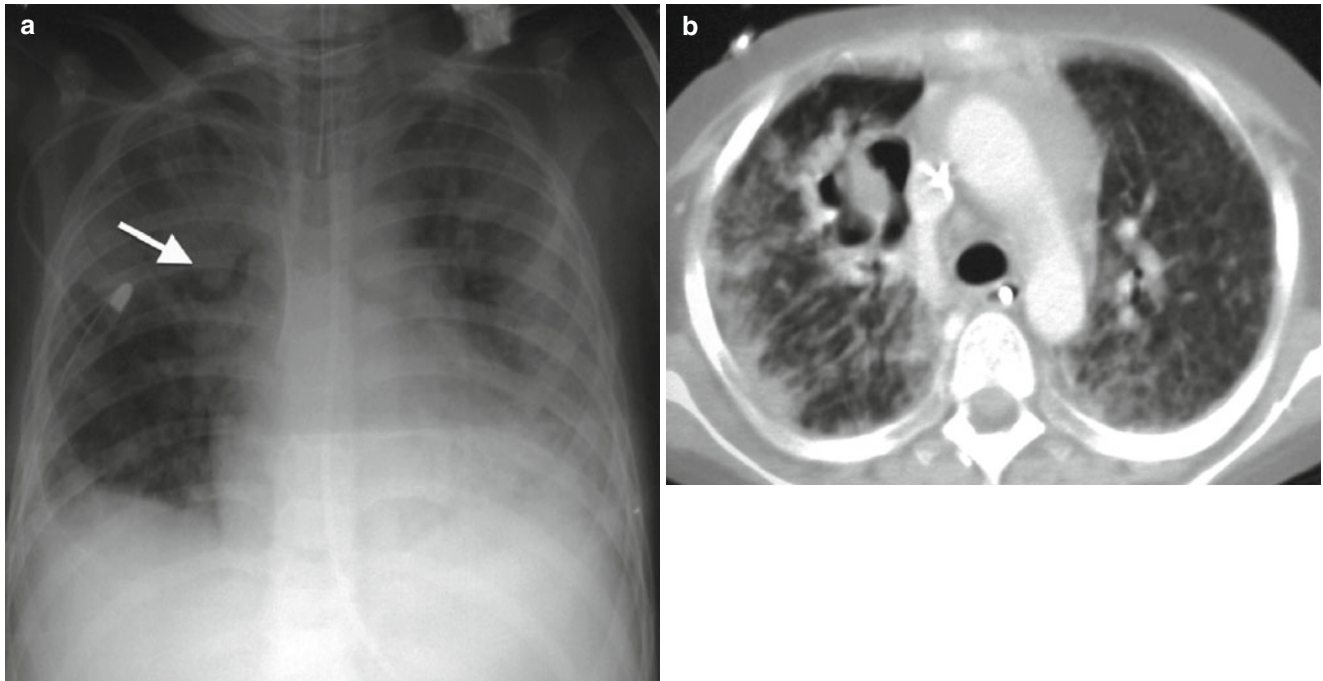
Fig. 13.29 Aspergillosis in the immunocompromised. Chest radiograph of a 3-year-old boy status post bone marrow transplant for leukemia (**a**) showing diffuse interstitial and alveolar disease with suspected cavity in the right upper lobe (*arrow*). Axial CT image (**b**) confirms the "air-crescent sign" of aspergillosis and the diffuse interstitial/alveolar disease

13.5.30 *Pneumocystis jiroveci* Infection
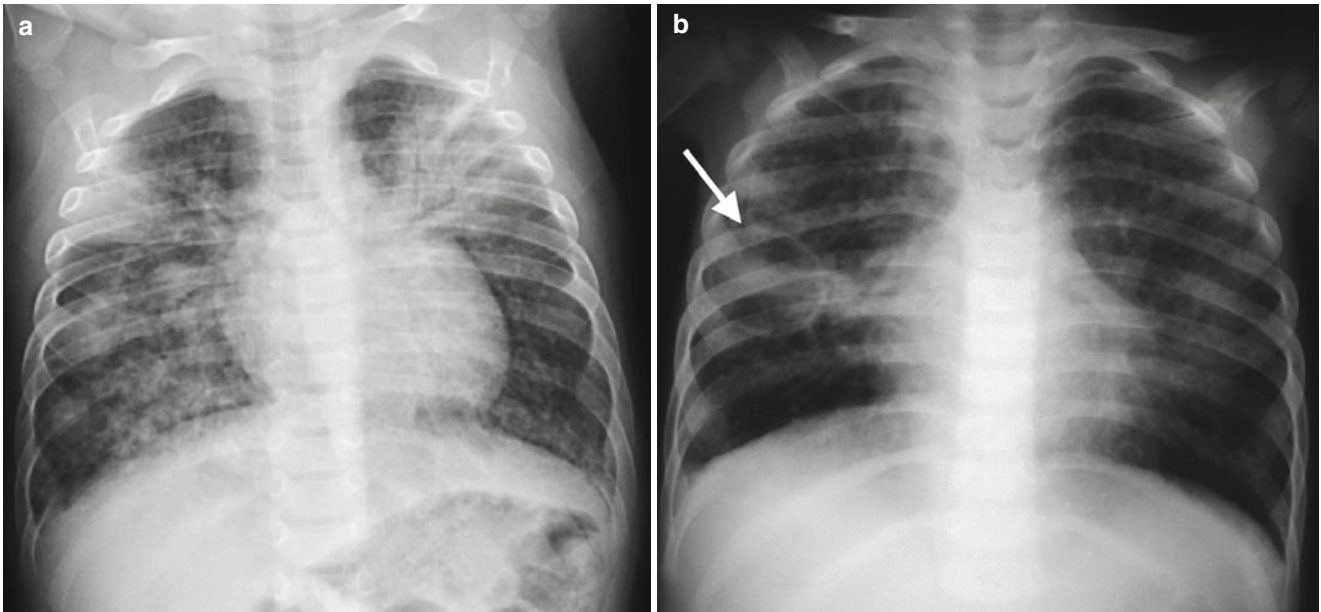
Fig. 13.30 *Pneumocystis jiroveci* infection. Radiograph of a 10-month-old boy diagnosed with severe combined immune deficiency syndrome showing diffuse reticulonodular interstitial pattern in both lungs with development of lung consolidations (**a**). Radiograph of a 14-month-old girl with HIV infection showing diffuse, bilateral interstitial lung pattern extending from the hilum (**b**). There is a cyst noted on the peripheral right lung (*arrow*)

References

Aherne W, Bird T, Court DS, et al. Pathological changes in virus infection of the lower respiratory tract in children. J Clin Pathol. 1970;23:7–18.

Berk SL, Verghese A. Parasitic pneumonia. Semin Respir Infect. 1998;3(2):172–8.

Blickman H (1998) Inflammatory lung disease, Chapter 2. In: Pediatric radiology, the requisites. 2ndedn. Mosby.

Bramson RT, Griscom NT, Cleveland RH. Interpretation of chest radiographs in infants with cough and fever. Radiology. 2005;236:22–9.

Collingsworth CL. Thoracic disorders in the immunocompromised. Radiol Clin North Am. 2005;43:435–47.

Condon VR. Pneumonia in children. J Thorac Imaging. 1991;6:31–44.

Czermak BV, Unsinn KM, Gotwald T, et al. *Echinococcus granulosus* revisited: radiologic patterns seen in pediatric and adult patients. AJR Am J Roentgenol. 2001;177:1051–6.

Daltro P, Santos EN, Gasparetto TD, et al. Pulmonary infections. Pediatr Radiol. 2011;41 Suppl 1:S69–82. doi:10.1007/s00247-0011-2012-8.

Donnelly LF. Maximizing the usefulness of imaging in children with community-acquired pneumonia. AJR Am J Roentgenol. 1999;172:505–12.

Donnelly LF. Practical issues concerning imaging of pulmonary infection in children. J Thorac Imaging. 2001;16:238–50.

Donnelly LF, Klosterman LA. Pneumonia in children: decreased parenchymal contrast enhancement-CT sign of intense illness and impending cavitary necrosis. Radiology. 1997;205:817–20.

Eslamy HK, Newman B. Pneumonia in normal and immunocompromised children: an overview and update. Radiol Clin North AM. 2011;49:895–920.

Foster K, Alton H. Chronic lung infection in children. Paediatr Respir Rev. 2003;4:225–9.

Hansell DM, Rubens MB, Padley SP, et al. Obliterative bronchiolitis: individual CT signs of small airways disease and functional correlation. Radiology. 1997;203:721–6.

Hodina M, Hanquinet S, Scnyder P, et al. Imaging of cavitary necrosis in complicated pneumonia. Eur Radiol. 2002;12(2):391–6. Epub 2001 Aug 28.

Hoffer FA, Bloom DA, Colin AA, et al. Lung abscess versus necrotizing pneumonia: implications for interventional therapy. Pediatr Radiol. 1999;29:87–91.

Houston S. Histoplasmosis and pulmonary involvement in the tropics. Thorax. 1994;49:598–601.

Hsieh SC, Kuo YT, Chern MS, et al. Mycoplasma pneumonia: clinical and radiographic features. Pediatr Int. 2007;49(3):363–7.

Jaffe A, Balfour-Lynn IM. Management of empyema in children. Pediatr Pulmonol. 2005;40:148–56.

Jeanes AC, Owens CM. Chest imaging in the immunocompromised child. Paediatr Respir Rev. 2002;3:59–69.

John SD, Ramanathan J, Swischuk LE. Spectrum of clinical and radiographic findings in pediatric mycoplasma pneumonia. Radiographics. 2001;21:121–31.

Kim WS, Moon WK, Kim IO, et al. Pulmonary tuberculosis in children: evaluation with CT. AJR. 1997;168:1005–9.

Kim JS, Ryu CW, Lee SI, et al. High resolution CT findings of varicella zoster pneumonia. AJR Am J Roentgenol. 1999;172:113–6.

Kim OH, Kim WS, Kim MJ, et al. Ultrasound in the diagnosis of pediatric chest diseases. Radiographics. 2000;20:653–71.

Kurt BA, Winterhalter KM, Connors RH, et al. Therapy of parapneumonic effusions in children: video-assisted thoracoscopic surgery versus conventional thoracostomy drainage. Pediatrics. 2006;118:547–53.

Lee EY, McAdam A, Chaudry G, Fishman M, et al. Swine-origin influenza A (H1N1) viral infection in children: initial chest radiographic findings. Radiology. 2010;254(3):934–41. doi:10.1148/radiol.09092083. Epub 2009 Dec 23.

Marais BJ, Gie RP, Schaaf HS, Hesseling AC, et al. The natural history of childhood intrathoracic tuberculosis: a critical review of prechemotherapy literature. Int J Tuberc Lung Dis. 2004;8:392–402.

Marks MJ, Haney PJ, McDermott MP, et al. Thoracic diseases in children with AIDS. Radiographics. 1996;16:1349–62.

McAdams HP, Rosado-de-Christenson ML, Lesar M. Thoracic mycoses from endemic fungi: radiologic-pathologic correlation. Radiographics. 1995;15:255–70.

Muller NL. Imaging of the pleura. Radiology. 1993;186:297–309.

Ostapchuk M, Roberts DM, Haddy R, et al. Community acquired pneumonia in infants and children. Am Fam Physician. 2004;70(5):899–908.

Paddock CD, Sanden GN, Cherry JD, et al. Pathology and pathogenesis of fatal bordetella pertussis infection in infants. Clin Infect Dis. 2008;47:328–38.

Perez-Velez CM, Marais BJ. Tuberculosis in children. N Engl J Med. 2012;367:348–61. doi:10.1056/NEJMra1008049.

Radkowski MA, Kranzler JK, Baem MO, et al. Chlamydia trachomatis in infants: radiography in 125 cases. AJR Am J Roentgenol. 1981;137(4):703–6.

Reittner P, Muller NL, Heyneman L, et al. Mycoplasma pneumoniae pneumonia: radiographic and HRCT features in 28 patients. AJR Am J Roentgenol. 2000;174:37–41.

Rose RE, Ward BH. Spherical pneumonias in children simulating pulmonary and mediastinal masses. Radiology. 1973;106:179–82.

Sakai S, Shida Y, Takahashi N, et al. Pulmonary lesions associated with visceral larva migrans due to *Ascaris suum* and *Toxocara canis*: imaging of six cases. AJR Am J Roentgenol. 2006;186:1697–702.

Santivanez S, Garcia HH. Pulmonary cystic echinococcosis. Curr Opin PulmMed.2010;16(3):257–61.doi:10.1097/MCP.0b013e3283386282.

Sarinas PS, Chitkara RK. Ascariasis and hookworm. Semin Respir Infect. 1997;12(2):130–7.

Swischuk LE, Hayden CK. Viral versus bacterial infections in children: is roentgenographic differentiation possible? Pediatr Radiol. 1986;16:278–84.

Tanaka N, Matsumoto T, Kuramitsu T, et al. High resolution findings in community acquired pneumonia. J Comput Assist Tomogr. 1996;20:600–8.

Thibodeau KP, Viera AJ. Atypical pathogens and challenges in community acquired pneumonia. Am Fam Physician. 2004;69(7):1699–706.

Westra SJ, Choy G. What imaging should we perform for the diagnosis and management of pulmonary infections? Pediatr Radiol. 2009;39 Suppl 2:S178–83.

Yalcin E, Dogru D, Haliloglu M, et al. Postinfectious bronchiolitis obliterans in children: clinical and radiological profile and prognostic factors. Respiration. 2003;70:371–5. doi:10.1159/000072900.